Author Manuscript

Title: Synergizing Electron and Heat Flows in Photocatalyst for Direct Conversion of Captured CO2

Authors: Chungseok Choi; Fengyi Zhao; James L Hart; Yuanzuo Gao; Fabian Menges; Conor L. Rooney; Nia J. Harmon; Bo Shang; Zihao Xu; Sa Suo; Quynh Sam; Judy J. Cha; Tianquan Lian; Hailiang Wang

To be cited as: 10.1002/anie.202302152

Link to VoR: https://doi.org/10.1002/anie.202302152

Synergizing Electron and Heat Flows in Photocatalyst for Direct Conversion of Captured CO_2

Chungseok Choi[1,2†], Fengyi Zhao[3†], James L Hart[4], Yuanzuo Gao[1,2], Fabian Menges[1], Conor L. Rooney[1,2], Nia J. Harmon[1,2], Bo Shang[1,2], Zihao Xu[3], Sa Suo[3], Quynh Sam[4], Judy J. Cha[4], Tianquan Lian[3], and Hailiang Wang[1,2*]*

[1]Department of Chemistry, Yale University, New Haven, CT 06511, United States. [2]Energy Sciences Institute, Yale University, West Haven, CT 06516, United States. [3]Department of Chemistry, Emory University, Atlanta, Georgia 30322, United States. [4]Department of Materials Science and Engineering, Cornell University, Ithaca NY 14853.

†These authors contributed equally to this work.

*To whom correspondence should be addressed: tlian@emory.edu; hailiang.wang@yale.edu

Abstract

We report a ternary hybrid photocatalyst architecture with tailored interfaces that boost the utilization of solar energy for photochemical CO_2 reduction by synergizing electron and heat flows in the photocatalyst. The photocatalyst comprises cobalt phthalocyanine (CoPc) molecules assembled on multiwalled carbon nanotubes (CNTs) that are decorated with nearly monodispersed cadmium sulfide quantum dots (CdS QDs). The CdS QDs absorb visible light and generate electron-hole pairs. The CNTs rapidly transfer the photogenerated electrons from CdS to CoPc. The CoPc molecules then selectively reduce CO_2 to CO. The interfacial dynamics and catalytic behavior are clearly revealed by time-resolved and *in situ* vibrational spectroscopies. In addition to serving as electron highways, the black body property of the CNT component can create local photothermal heating to activate amine-captured CO_2, namely carbamates, for direct photochemical conversion without additional energy input.

Introduction

The photochemical CO_2 reduction reaction is an emerging way to convert abundant and clean solar energy into chemical energy and simultaneously remedy the earth from increasing carbon emissions. Critical steps for photochemical CO_2 reduction include generation of electron-hole pairs, transfer of electrons to catalytically active sites, and catalytic CO_2 reduction.[1-3] To meet these requirements, a semiconductor material is needed to efficiently convert photons to electron-hole pairs under sunlight illumination; the photo-generated electrons should be quickly transferred to catalytic sites that have a suitable binding affinity for CO_2 and a sufficient reduction potential to reduce CO_2. Among all semiconductors, CdS is a proper candidate with a bandgap in the visible region (~ 43% energy of the solar spectrum) and a sufficiently high conduction band minimum that suits CO_2 photoreduction.[4] While several structural modification approaches have been reported for improving the photochemical CO_2 reduction performance of CdS,[5,6] current CdS-based photocatalytic systems are still limited by fast electron-hole recombination, slow electron transfer to catalytic sites, and insufficient CO_2 reduction activity.[7] Ideally, an effective electron transfer component connecting the light absorber with a highly active CO_2 reduction catalyst would address these issues. However, realizing such a photocatalyst architecture is a notable challenge as it requires solving physical and chemical problems at multiple material interfaces.[7]

Practical photochemical CO_2 valorization will have to take CO_2 capture into consideration. Lewis base molecules like alkyl amines are well-known absorbents that can effectively capture CO_2 by forming carbamates.[8] However, regenerating CO_2 from carbamate solutions for CO_2 utilization usually requires extensive heating, which is energy-demanding and may produce toxic byproducts.[9] Direct conversion of a carbamate to yield CO_2 reduction products and simultaneously regenerate the amine would be an ideal approach to integrated CO_2 capture and utilization. However, these reactions are challenging because additional energy is required to break the C-N bond in the carbamate.[10-12] In consideration of this need, a smart design of CO_2 reduction photocatalyst materials might be to incorporate a component that can photothermally liberate or activate CO_2 from its carbamate form near the CO_2 reduction catalytic sites.

In this work, we developed a ternary hybrid photocatalyst material, consisting of CdS quantum dots (QDs) and cobalt phthalocyanine (CoPc) molecules selectively anchored on multiwalled carbon nanotubes (CNTs), that addresses all the aforementioned challenges. In this material architecture, CdS is the light absorber, CoPc is the CO_2 reduction catalyst with known activity and selectivity for CO production like several other metal phthalocyanines and porphyrins,[13-17] and CNT serves as a charge transfer highway between CdS and CoPc. The intimate CdS/CNT and CNT/CoPc interfaces resulting from well-controlled material synthesis significantly accelerate charge carrier separation in the light absorber and electron transfer to the catalytic sites through the highly conductive CNTs. Our

photocatalyst delivers a high CO production rate of 6.3 μmol h^{-1} (6.3 mmol g^{-1} h^{-1}) under visible light illumination. Remarkably, the photothermal effect of CNT enables local heating near the photocatalyst, which makes carbamate reactive. Taking advantage of this property, we successfully demonstrated direct photochemical production of CO from CO_2 captured by monoethanolamine (MEA) from air.

Results and Discussion

The CdS/CNT/CoPc ternary hybrid material was synthesized by firstly growing CdS QDs on multiwalled CNTs and subsequently assembling CoPc molecules on the uncovered CNT surfaces. We reacted cadmium (II) oleate with elemental sulfur in the presence of CNTs, oleic acid (OA) and oleylamine in octadecene at 140 °C to form CdS/CNT. The reaction temperature was controlled to be considerably lower than typical CdS QD syntheses (~ 250 °C) to allow for selective nucleation and growth of QDs on CNT surfaces.[18] OA served as a capping agent to control the size of CdS QDs. Transmission electron microscopy (TEM) characterization of CdS/CNT/CoPc revealed that nanoparticles with a narrow size distribution are selectively and uniformly anchored on CNT surfaces (Figure S1). Scanning transmission electron microscopy recorded with a high-angle annular dark-field detector (STEM-HAADF) clearly showed spherical nanoparticles with a diameter of ~ 5 nm on CNTs (Figure 1a). X-ray diffraction (XRD) confirmed the successful synthesis of CdS in the zinc blende phase (Figure 1b). The hybrid material shows two absorption peaks in the UV-visible spectrum at 480 nm and 660 nm (Figure 1c), characteristic of CdS QDs and CoPc, respectively.[15,19] Elemental mapping by electron energy loss spectroscopy (EELS) visualized CNTs and CdS QDs in the hybrid structure (Figure 1d-g). Notably, a layer of C is visible on the surface of the CdS QDs (red box in Figure 1e), which reflects the surface ligands. This OA capping layer may help suppress the toxicity of CdS as opposed to previous studies which mostly used uncapped CdS photocatalysts.[20,21]

CoPc molecules were assembled onto the uncovered CNT surfaces of CdS/CNT via non-covalent π-π interaction. High-resolution STEM-HAADF imaging of CdS/CNT/CoPc showed dispersion of high-contrast atoms (heavy metal atoms such as Co) on CNTs (Figure 1h). Energy dispersive X-ray (EDX) spectroscopy analysis confirmed the presence of Co element in CdS/CNT/CoPc but not in bare CNTs (Figure S2), which verifies the effective loading of CoPc. Inductively coupled plasma mass spectrometry (ICP-MS) revealed that the hybrid material contains approximately 70 wt% of CdS, 30 wt% of CNT, and 0.15 wt% of CoPc. These characterization results together delineate the structure of the CdS/CNT/CoPc ternary hybrid material as illustrated in Figure 1i.

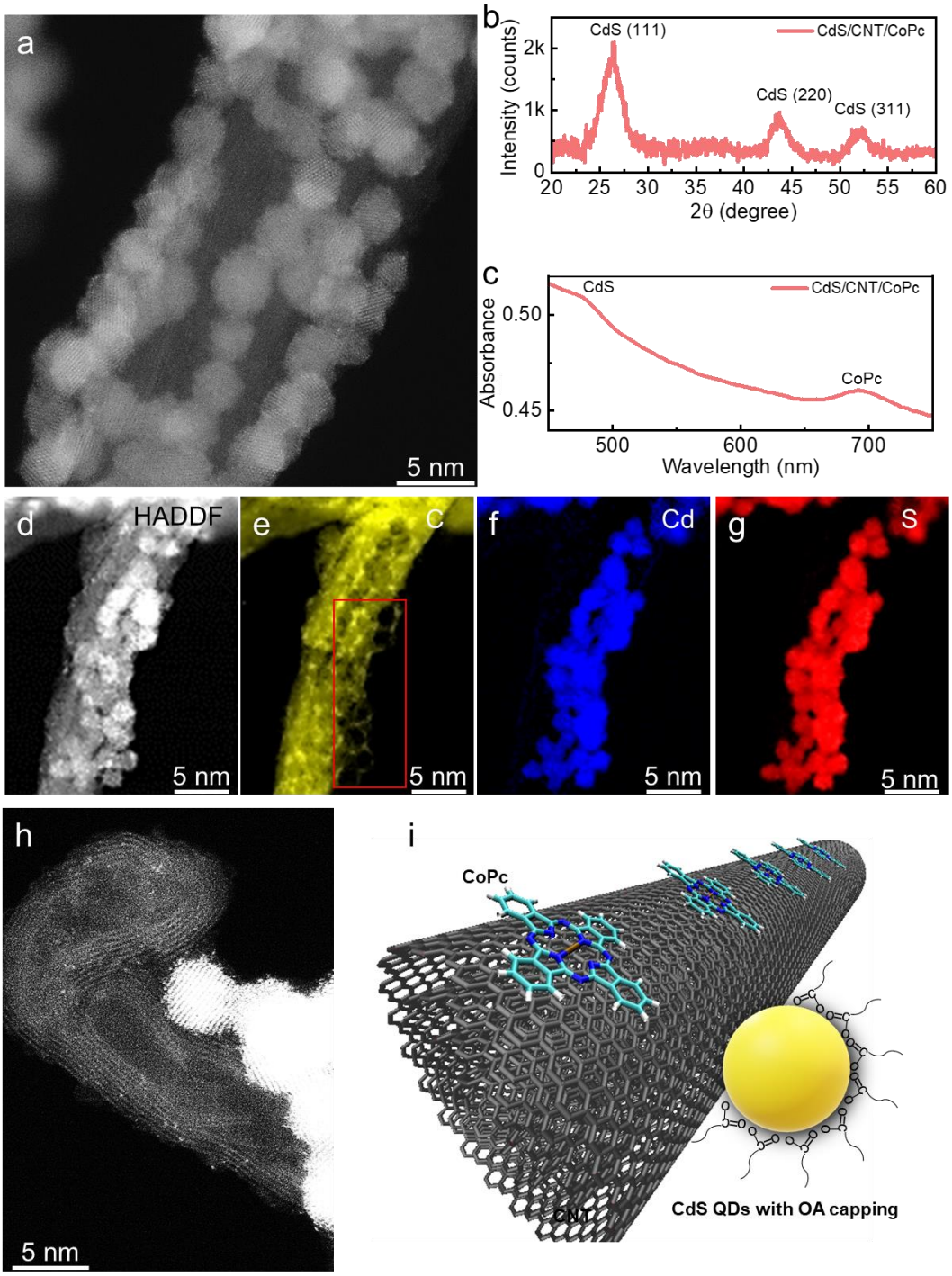

Figure 1. CdS/CNT/CoPc hybrid material. a, STEM-HAADF image of CdS/CNT/CoPc. **b**, XRD of CdS/CNT/CoPc. **c**, UV-visible spectroscopy of CdS/CNT/CoPc. **d-g**, STEM-HAADF image and EELS elemental mapping of CdS/CNT/CoPc. **h**, High-resolution STEM-HAADF image of CdS/CNT/CoPc. **i**, Schematic illustration of CdS/CNT/CoPc structure.

Additional characterization was performed to understand the electronic structure of the ternary hybrid photocatalyst (Table S1). Cyclic voltammetry was used to determine the redox levels of CoPc and their

positions with respect to the standard electrode potential of CO_2/CO (Figure S3). The first reduction level is 0.07 eV below CO_2/CO, and the second reduction is 0.5 eV higher (Figure 2). The energy gap corresponding to the Q band of CoPc was determined to be 1.78 eV from the Tauc plot (Figure S4). Ultraviolet photoelectron spectroscopy (UPS) was carried out to determine the work function of CNT as 4.09 eV (Figure S5) and the valence band maximum of CdS as 1.99 eV below the Fermi level of CNT (Figure S6). The band gap of the CdS QDs was measured from the Tauc plot to be 2.45 eV (Figure S7 and S8). These results allowed us to draw a wholistic energy band diagram of the CdS/CNT/CoPc ternary hybrid photocatalyst as shown in Figure 2. On the light absorber side, the conduction band of CdS QDs is high enough to generate electrons with sufficient reducing power for CO_2 conversion to CO. These electrons can be easily transferred to CNTs. On the co-catalyst side, CoPc needs to be doubly reduced to be active for reducing CO_2 to CO, which is consistent with the understanding from our prior electrocatalytic studies.[22] However, the second reduction energy level of CoPc is 0.26 eV higher than the Fermi level of CNTs, which indicates that electron accumulation in CNTs is required to further inject electrons into singly reduced CoPc.

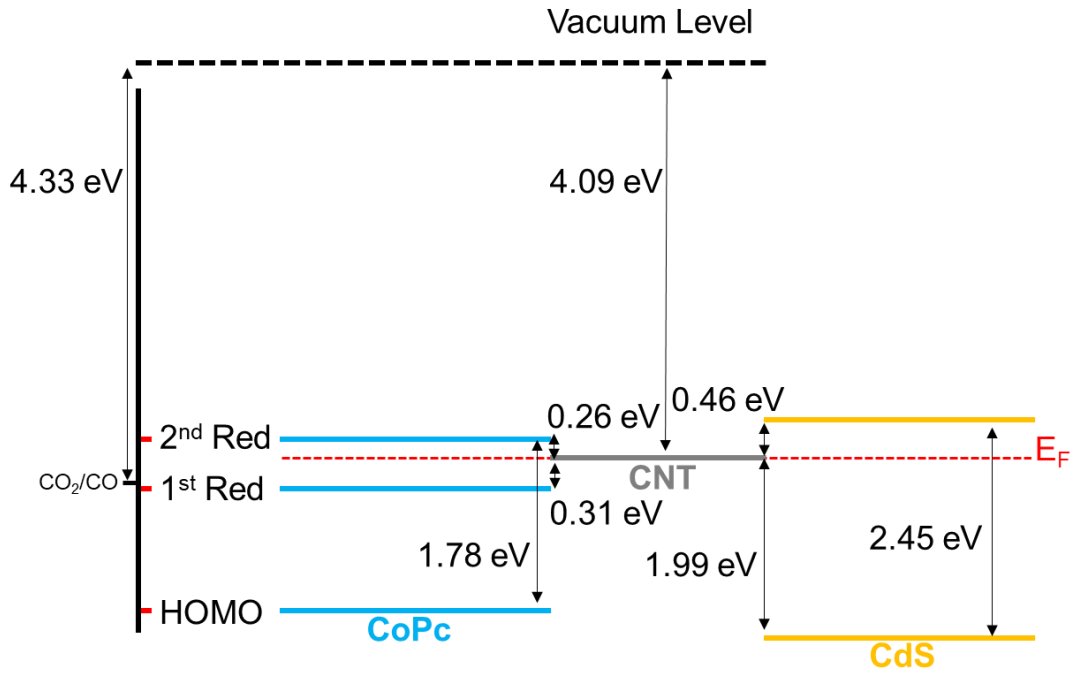

Figure 2. Electronic energy level diagram of CdS/CNT/CoPc.

Transient absorption (TA) spectroscopy was carried out to study the photo-induced charge separation process in the CdS/CNT/CoPc hybrid photocatalyst (Figure S9). Upon 400 nm excitation, CdS QDs, CdS/CNT and CdS/CNT/CoPc all exhibited a signal bleach centered at ~ 475 nm (Figure 3a, b, and Figure S10), which is related to the state-filling effect of the first exciton transition of CdS. As has been

shown previously, the amplitude of the CdS exciton bleach can be directly related to the population of excited electrons at the CdS conduction band edge and can be used to follow the kinetics of electron-hole recombination and interfacial electron transfer.[23,24] This measurement was performed with power density within the single exciton region identified from the plot of maximum bleach signal recorded at 1 ps vs excitation power density (Figure S11) to avoid complication from multi-exciton Auger recombination in CdS QDs. CdS/CNT showed a higher single exciton threshold power density than CdS QDs, which is attributed to the absorption and scattering by the CNTs that leads to decreased photon absorption of CdS under the same power density.

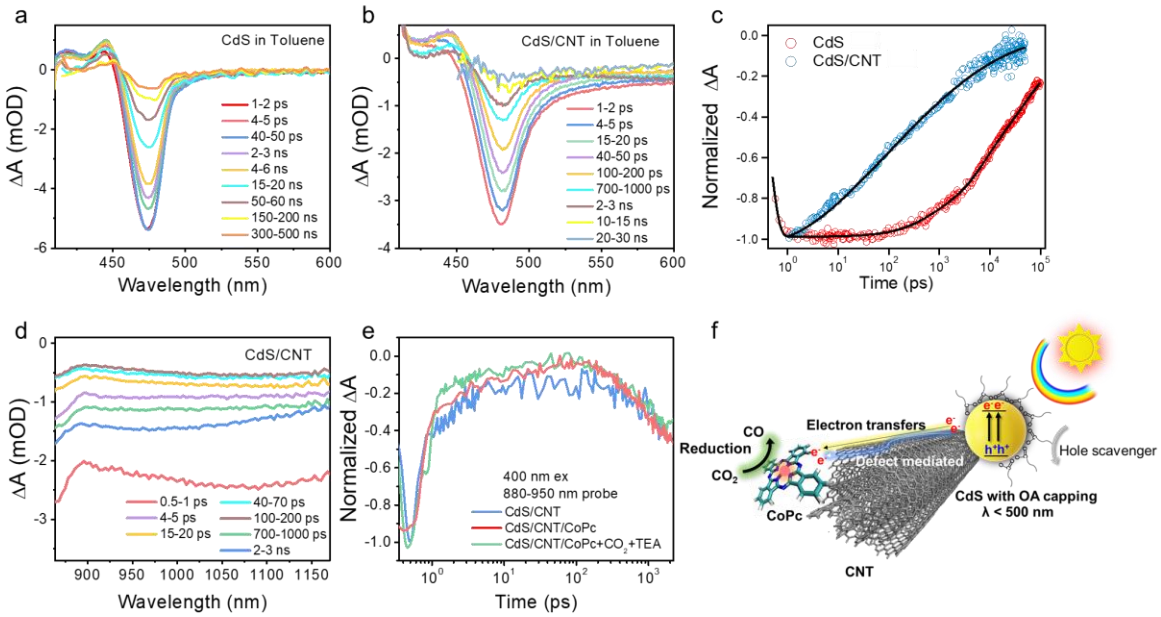

Figure 3. Electron transfer kinetics. TA spectra (400 nm excitation) probing CdS exciton bleach signal for (**a**) CdS QDs and (**b**) CdS/CNT at varied time delays. **c**, Comparison of normalized exciton bleach signal decay between CdS/CNT and CdS QDs. Signal was averaged from 468 nm to 483 nm. Black curves are fitting results using Equations S2 and S3. **d**, Near-IR TA spectra (400 nm excitation) probing CNT bleach signal for CdS/CNT. **e**, CNT bleach kinetics of CdS/CNT and CdS/CNT/CoPc. Signal was averaged from 880 nm to 950 nm. **f**, Proposed electron transfer pathway.

The exciton bleach signal of CdS/CNT showed a faster decay than free CdS QDs without CNT (Figure 3c), suggesting the transfer of excited electrons from CdS to CNT. The exciton bleach recovery kinetics of the CdS QDs can be fitted by a multi-exponential decay equation with an average lifetime of 168±24 ns (Table S2 and Equations S2, S4). This non-single-exponential decay of the exciton bleach signal has been attributed to the recombination of electrons in the conduction band with holes in the trap states of CdS.[25] The exciton bleach kinetics of CdS/CNT can be best fitted by a stretched exponential decay function (Table S2 and Equation S3), which describes the kinetics of charge transfer from CdS to CNT via a dispersive transport model.[26-28] The fitting results are summarized in Table S2.

The dramatic difference in exciton average lifetime between CdS/CNT and CdS QDs reflects a ~ 37 times faster interfacial electron transfer rate in CdS/CNT than the electron-hole charge recombination rate within CdS. From the exciton bleach decay kinetics shown in Figure 3c, the electron transfer quantum yield QE_{ET} can be calculated to be 76.6 % using a previously proposed model (Equation S6).[29] The rapid electron transfer from CdS to CNT is also supported by our observation of no difference in decay kinetics within the first 5 ns when a hole scavenger, triethylamine (TEA), was introduced into the system (Figure S12a). CdS/CNT/CoPc showed the same exciton bleach kinetics as CdS/CNT without CoPc (Figure S12b). This indicates that the charge transfer from CNT to CoPc occurs on a much slower timescale and has no effects on the initial charge separation. It also rules out the possibility of direct electron transfer from CdS to CoPc molecules in the CdS/CNT/CoPc hybrid material. Thus, the observed fast exciton bleach signal decay for CdS/CNT is mainly attributed to the rapid electron transfer from CdS to CNT upon the excitation of CdS.

TA spectra in the near-IR region were used to characterize the arrival kinetics of electrons to CNT in the hybrid photocatalyst. Upon excitation, we observed a broad negative signal in the 870 – 1175 nm region for both CdS/CNT (Figure 3d) and pure CNTs (Figure S13a), which is assigned to the bleach of the M11 transition of metallic CNTs.[30-31] The wide size distribution of the CNTs is likely responsible for the broad signal. The decay kinetics of CNTs can be fitted by a single exponential function with a time constant of 171 ± 9 fs (Figure S13b), indicating fast carrier relaxation due to electron-phonon scattering.[31-33] Interestingly, the bleach signal of CdS/CNT upon 400 nm excitation exhibits complex kinetics consisting of a decay component from 0 to 100 ps and then a gradual increase component from 100 ps to 2 ns (Figure 3d, e) in addition to the sub-picosecond decay observed for CNTs alone. This kinetics can be explained by the model proposed in Figure S14c and Equation S10. Briefly, the first term in Equation S10 describes the sub-picosecond decay component, which can be fitted with the same instantaneous rise and sub-picosecond decay time constants of the signal observed for pure CNTs and can be attributed to carrier dynamics resulted from the direct excitation of CNTs by 400 nm light. This assignment is further supported by the observation of the same fast decay kinetics in CdS/CNT excited by 800 nm light (Figure S14a), which selectively excites the CNT (and not the CdS) component. The second and third terms describe the kinetics of electron transfer from CdS QDs to the subpopulations of CNTs with and without electron traps, respectively. In CNTs with electron traps, due to an electron trapping time (0.14 ps) that is much faster than the interfacial electron transfer from CdS, the electron population (the bleach amplitude) grows on the electron trapping time scale and decays on the time scale of electron transfer, which accounts for the decay component on the sub-picosecond to 100 ps time scale in Figure 3e. In CNTs with negligible numbers of electron traps, the electron population grows with the electron transfer kinetics, which accounts for the bleach signal growth on the 100 ps to 2 ns time scale in Figure 3e. The details of the fitting model are described in Equation S10 and the fitting parameters are listed in Table S3. This model, with a clear physical meaning (Figure S14c) that

is consistent with the experimentally measured energy levels (Figure 2), provides a satisfactory fit to the observed complicated kinetics (Figure S14a), which supports electron accumulation in the CNTs of CdS/CNT/CoPc under illumination (excitation of CdS). The accumulated electrons in CNT can raise its Fermi level and enable electron transfer to the second reduction state of CoPc (Figure S14c and Figure 2). No difference in kinetics between CdS/CNT and CdS/CNT/CoPc was observed (Figure 3e) since the reduction of CoPc takes place on a much slower timescale. Adding TEA also made no difference (Figure 3e), indicating that no back recombination takes place between separated electrons in CNTs and holes in CdS within the 5 ns time range.

The photocatalytic performance of CdS/CNT/CoPc for CO_2 reduction was tested in acetonitrile with triethanolamine (TEOA) as the electron donor under the illumination of an AM1.5G-filtered 150 W Xe lamp (216 mW cm^{-2} beam power). The ternary hybrid photocatalyst exhibited a high CO production rate of 3.1 μmol h^{-1} (3.1 mmol g^{-1} h^{-1}) and a high CO/H_2 ratio of 93% (Figure 4a). Replacing Ar for CO_2 generated no CO (Figure 4a), and an isotope labeling experiment with $^{13}CO_2$ yielded ^{13}CO almost exclusively (Figure S15), both confirming that CO is indeed produced from CO_2 reduction. Controlled experiments with CdS/CNT and CNT/CoPc binary hybrids both produced no CO (Figure 4a), suggesting that both CdS and CoPc are critical components of the ternary photocatalyst. The result that CNT/CoPc has no photocatalytic activity rules out the possibility that CoPc molecules are excited to generate electrons for CO_2 reduction. Another binary material CdS/CoPc (Figure S7) showed a substantially lower CO production rate (0.1 μmol h^{-1}) compared to the ternary hybrid (Figure 4a), which reflects the critical role of CNT facilitating charge separation in CdS and electron transfer to the CoPc co-catalyst.

The intimate and abundant interface between CdS and CNT in the ternary hybrid, as rendered by the direct growth of CdS QDs on CNTs, is critical to the charge separation and transfer.[34,35] To test this hypothesis, we prepared another CdS/CNT/CoPc material by assembling CoPc molecules on pre-heated CdS/CNT. The pre-heating at 150 °C caused the CdS QDs to detach from the CNTs and sinter into larger particles, destroying the CdS/CNT interface (Figure S16a, b). The UV-visible spectrum of this heated CdS/CNT/CoPc material features a ~ 40 nm redshift of the CdS absorption peak, consistent with CdS aggregation, and a CoPc absorption peak confirming effective loading of CoPc (Figure S16c). Notably, the CdS/CNT/CoPc material with aggregated CdS showed drastically lower CO_2 reduction photocatalytic activity than the original ternary hybrid (Figure 4a), verifying the vital role of the CdS/CNT interface in the ternary material system.

Photocatalytic CO_2 reduction performance of CdS/CNT/CoPc was also tested under visible light illumination. With a 405 nm LED (47 mW cm^{-2} beam power) light source, a high CO production rate of 2.9 μmol h^{-1} (2.9 mmol g^{-1} h^{-1}) was achieved and maintained for at least 5 hours (Figure 4b). The ~ 1 hour pre-activation time may be related to electron accumulation in CNTs for overcoming the 0.26 eV

energy barrier between the 2nd reduction of CoPc and the CNT Fermi level (Figure 2) or to the multiple reductions of CoPc required for CO_2 activation.[15] When we replaced the light source to a UV-filtered 300 W Xe lamp (618 mW cm^{-2} beam power), the CO production rate increased to 6.3 μmol h^{-1} (6.3 mmol g^{-1} h^{-1}), marking one of the highest rates reported up to date under visible light at room temperature (Table S4).

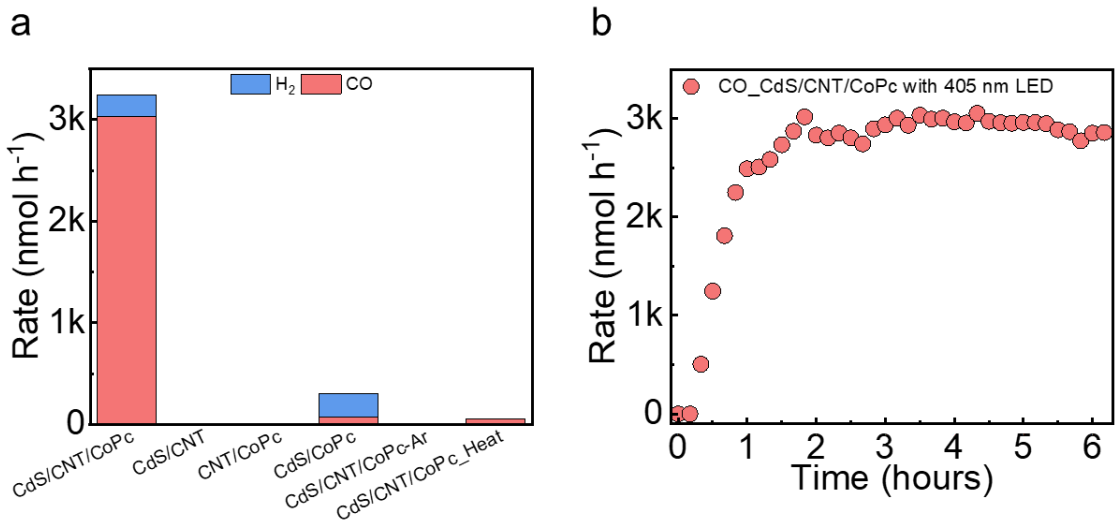

Figure 4. Photocatalytic CO_2 reduction performance measured in TEOA-acetonitrile (1:4). a, Photocatalytic reaction rate of CdS/CNT/CoPc compared to CdS/CNT, CNT/CoPc, and CdS/CoPc under AM1.5G-filtered 150 W Xe lamp illumination (216 mW cm^{-2} beam power). **b**, Long-term photocatalytic CO production rate of CdS/CNT/CoPc under 405 nm LED illumination (47 mW cm^{-2} beam power).

In situ Raman spectroscopy was conducted to identify CO_2 reduction active sites in the CdS/CNT/CoPc photocatalyst (Figure S17). In the first experiment, we used methyl viologen (MV^{2+}) as an electron acceptor.[36] Under 405 nm LED illumination, we observed MV^{2+} reduction to MV^{+} in the presence of CdS/CNT/CoPc but not with CdS/CNT (Figure 5a). This difference suggests that CoPc is the catalytically active site that transfers photo-generated electrons to oxidant molecules. In the second experiment, we performed photochemical CO_2 reduction with CdS/CNT/CoPc. Under illumination and CO_2 atmosphere, we observed Raman features at 590 cm^{-1}, 682 cm^{-1}, 749 cm^{-1}, and 1532 cm^{-1}, characteristic of $Co^{2+}Pc^{2-}$ (or $Co^{+}[HPc]^{-}$) molecules (Figure 5b).[37] All these Raman peaks disappeared after changing the gas atmosphere from CO_2 to Ar. This is caused by the reduction of CoPc, likely to $Co^{+}[H_2Pc]^{-}$, which bleaches the color of the molecule and consequently disrupts its resonance with the 633 nm Raman laser.[15] Notably, the CoPc peaks returned when Ar was again replaced by CO_2, indicating that $Co^{+}[H_2Pc]^{-}$ can quickly transfer electrons to CO_2 and is therefore the active species in the photochemical CO_2 reduction catalyzed by CdS/CNT/CoPc. This is consistent with our prior

electrochemical CO_2 reduction study, which indicates CoPc needs to be reduced by two electrons before it can actively reduce CO_2 to CO.[22]

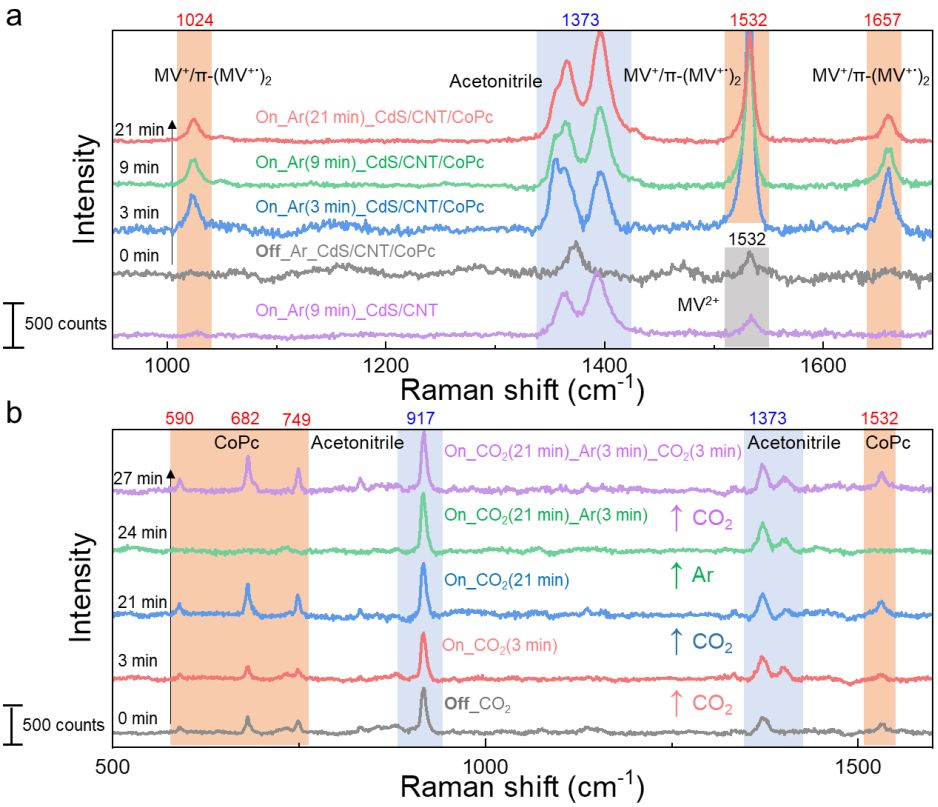

Figure 5. *In situ* Raman spectroscopy measurements to uncover catalytic sites and electron transfer. *In situ* Raman spectra of CdS/CNT/CoPc in TEOA-acetonitrile (1:4) under photochemical conditions (405 nm LED illumination) (**a**) with MV^{2+} or (**b**) CO_2 as electron acceptor.

The electron transfer from CoPc to CO_2 was further probed by *in situ* UV-visible spectroscopy with CdS/CNT/CoPc (Figure S18). Under Ar atmosphere without illumination, an absorption peak at 669 nm corresponding to $Co^{2+}Pc^{2-}$ was observed (Figure 6a).[15,38,39] 30 min after turning on the 405 nm LED, the 669 nm peak disappeared, and two new peaks emerged at 660 nm and 698 nm, reflecting Co^{2+} reduction to Co^{+}.[15,38,39] After 60 min of illumination, the 660 nm peak started to disappear, whereas the 698 nm one continued to grow, and two additional peaks started to emerge at 423 nm and 466 nm (Figure 6a). These changes suggest the second reduction of CoPc, likely from $Co^{+}[HPc]^{-}$ to $Co^{+}[H_2Pc]^{-}$ (reduction of the ligand).[15,38,39] The approximately 1 hour of time needed to generate the CO_2-reduction-active $Co^{+}[H_2Pc]^{-}$ species matches well with the activation time of the aforementioned photochemical CO_2 reduction measurement (Figure 4b), which may be related to electron accumulation in the CNTs to overcome the 0.26 eV energy barrier shown in Figure 2.

We then conducted the experiment under CO_2 atmosphere. Interestingly, after the initial reduction, the CoPc molecular catalyst manifested a mixed state of $Co^+[HPc]^-$ and $Co^+[H_2Pc]^-$ with their ratio fluctuating in the following 2 hours (Figure 6b). This indicates the two redox states of CoPc involved in the catalytic cycle of CO_2 reduction: photo-generated electrons from CdS reduce CoPc to $Co^+[H_2Pc]^-$, which is subsequently oxidized by CO_2 to form $Co^+[HPc]^-$. To prove this conjecture, we first photo-reduced CdS/CNT/CoPc under Ar to form $Co^+[H_2Pc]^-$ and then dosed CO_2 into the system. CO_2 converted $Co^+[H_2Pc]^-$ to $Co^+[HPc]^-$ almost immediately (Figure 6c), which is consistent with the aforementioned *in situ* Raman results and confirms our hypothesis about the active form of CoPc and its electron transfer to CO_2 in the photochemical reaction.

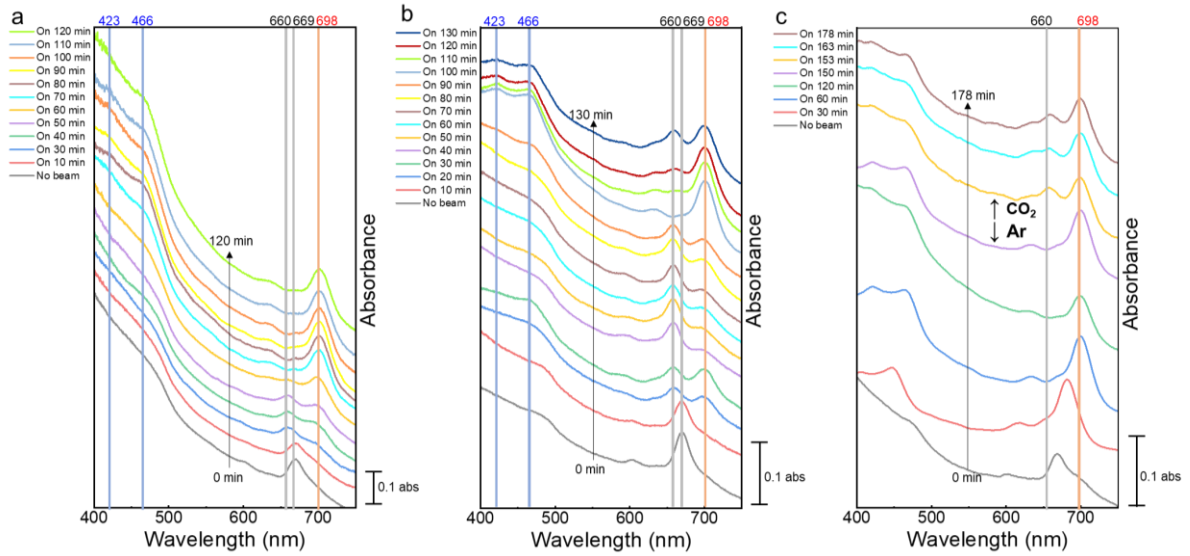

Figure 6. *In situ* UV-visible spectroscopy measurements to uncover catalytic sites and electron transfer. *In situ* UV-visible spectra of CdS/CNT/CoPc in TEOA-acetonitrile (1:4) under photochemical conditions (405 nm LED illumination), (**a**) with Ar purging, (**b**) with CO_2 purging, and (**c**) with first Ar and then CO_2 purging.

An important aspect of CO_2 utilization is its integration with CO_2 capture. Amine solutions are widely used to absorb CO_2 by forming carbamates, but a considerable amount of energy, usually in the form of heat, is needed to release the captured CO_2 for valorization.[12] The black body characteristic of CNTs in our CdS/CNT/CoPc ternary hybrid photocatalyst enables it to absorb solar irradiation and generate heat,[40] which may be used towards overcoming the energy barrier for releasing CO_2 from carbamate and realize the direct photochemical conversion of captured carbon emissions. To this goal, we first carried out photochemical CO_2 reduction in 0.2 M aqueous MEA with our CdS/CNT/CoPc catalyst. The CO_2 in this MEA solution was captured from bubbling CO_2 gas through the solution, which yielded a carbamate concentration of ~ 6.8 mM (Figure S19). Under the illumination of a 300 W Xe lamp (766 mW cm^{-2} beam power), the reaction produced CO at a notable rate of 1.2 µmol h^{-1} together with 21

μmol h^{-1} of H_2 (Figure 7a). The H_2 production rate is inversely related with the carbamate concentration (Figure S20), which provides an opportunity to adjust the CO/H_2 ratio in the valuable syngas product. Controlled experiments without the CoPc co-catalyst, without the CdS/CNT/CoPc photocatalyst, or without captured CO_2 all showed background level CO production rates. Isotope labeling experiments with $^{13}CO_2$ confirmed ^{13}CO production from the carbamate source (Figure S21). To further push the performance of our system, we captured CO_2 from the ambient atmosphere using 0.2 M MEA, which yielded a carbamate concentration of ~ 2.2 mM (Figure S19). Remarkably, our CdS/CNT/CoPc hybrid catalyst effectively reduced carbamate photochemically to CO at a rate of 0.3 μmol h^{-1}, significantly higher than the background signal (Figure 7b). We observed that a considerable amount of heat was released by the CdS/CNT/CoPc photocatalyst during the reactions (Figure S22). A simplified simulation with COMSOL estimated a local temperature of ~ 50 °C near the catalyst (Figure 7c). This value agrees with what was found necessary for carbamate solutions to be electrochemically reactive.[12] Therefore, the photothermal effect of CNT in our ternary hybrid photocatalyst provides local heating, without the need for additional energy input, to make carbamate reactive towards photochemical reduction (Figure 7d). To the best of our knowledge, this is the first demonstration of direct photochemical conversion of amine-captured CO_2 with no additional energy input, although more optimization is still needed to advance it towards practical application.

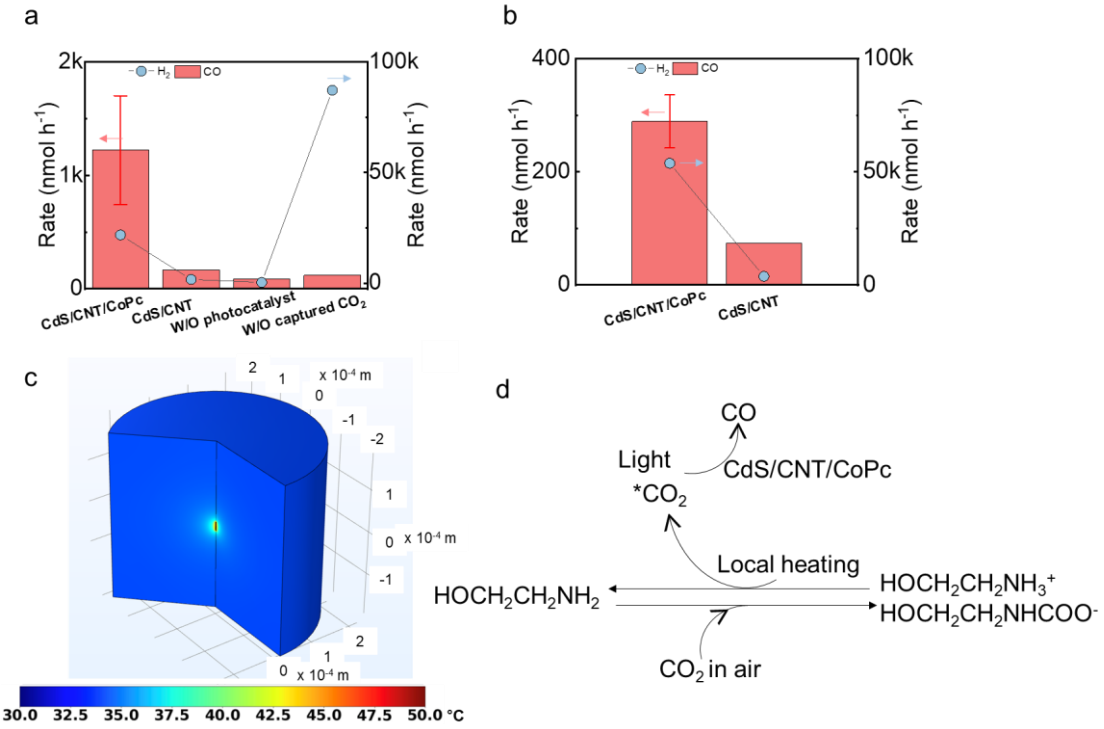

Figure 7. Photocatalytic conversion of captured CO_2. Photochemical CO and H_2 production from CO_2 captured by MEA solution (**a**) from a pure CO_2 source and (**b**) from air catalyzed by CdS/CNT/CoPc. **c**, Modeling of local heating effect near CNT. **d**, Proposed mechanism for direct photocatalytic reduction of MEA-captured CO_2.

Conclusion

This study develops a ternary CdS/CNT/CoPc hybrid photocatalyst towards utilizing solar energy for practical CO_2 valorization. CdS QDs in the hybrid material exhibit effective electron-hole pair generation under visible light irradiation. CNT with intimate CdS/CNT and CNT/CoPc interfaces rapidly transfers photogenerated electrons from CdS to CoPc which efficiently reduces CO_2 to CO. In addition, the photothermal effect of CNT in the hybrid catalyst structure enables direct photochemical conversion of amine-captured CO_2.

Acknowledgment: This work was supported as part of the Center for Hybrid Approaches in Solar Energy to Liquid Fuels (CHASE), an Energy Innovation Hub funded by the U.S. Department of Energy, Office of Science, Office of Basic Energy Sciences under Award Number DE-SC0021173 (T.L. and H.W.). STEM work was supported by U.S. National Science Foundation Grant #1749742 (J.J.C.).

References:

1. S. Xie, Q Zhang, G. Liu, *Chem. Commun*. **2016**, *52*, 35-59.
2. S. Sato, T. Morikawa, S. Saeki, T. Kajino, T. Motohiro, *Angew. Chem.* **2010**, *122*, 5227-5231.
3. R. Kuriki, K. Sekizawa, O. Ishitani, K. Maeda, *Angew. Chem.* **2015**, *54*, 2406-2409.
4. L. Cheng, Q. Xiang, Y. Liao, H. Zhang. *Energy Environ. Sci.* **2018**, *11*, 1362-1391.
5. M. Zhou, S. Wang, P. Yang, C. Huang, X. Wang, *ACS Catal.* **2018**, *8*, 4928-4936.
6. M. Kuehnel, K. L. Orchard, K. E. Dalle, E. Reisner, *J. Am. Chem. Soc.* **2017**, *139*, 7217-7223.
7. K. Yang, Z. Yang, C. Zhang, Y. Gu, J. Wei, Z. Li, C. Ma, X. Yang, K. Song, Y. Li, Q. Fang, *Chem. Eng. J.* **2021**, *418*, 129344.
8. G. T. Rochelle, *Science* **2009**, *325*, 1652-1654.
9. R. S. Haszeldine *Science* **2009**, *325*, 1647-1652.
10. J. H. Rheinhardt, P. Singh, P. Tarakeshwar, D. A. Buttry. *ACS Energy Lett.* **2017**, *2*, 454-461.
11. G. S. Hwang, H. M. Stowe, E. Paek, D. Manogaran, *Phys. Chem. Chem. Phys.* **2015**, *17*, 831-839.
12. G. Lee, Y. C. Li, J. Y. Kim, T. Peng, D. H. Nam, A. Sedighian Rasouli, F. Li, M. Luo, A. H. Ip, Y. C. Joo, E. H. Sargent, *Nat. Energy* **2021**, *6*, 46-53.
13. Z. Liang, H. Y. Wang, H. Zheng, W. Zhang, R. Cao, *Chem. Soc. Rev.* **2021**, *50*, 2540-2581.
14. R. Cao. *ChemSusChem*, **2022**, *15*, e202201788.
15. B. Shang, F. Zhao, C. Choi, X. Jia, M. Pauly, Y. Wu, Z. Tao, Y. Zhong, Z. Harmon, P. A. Maggard, T. Lian, N. Hazari, H. Wang, *ACS Energy Lett.* **2022**, *7*, 2265-2272.
16. Y. Wu, Y. Liang H. Wang, Acc. Chem. Res. **2021**, *54*, 3149-3159.
17. X. Lu, Y. Wu, X. Yuan, L. Huang, Z. Wu, J. Xuan, W. Yifei, H. Wang, *ACS Energy Lett*. **2018**, *3*, 2527-2532.
18. L. Huang, X. Wang, J. Yang, G. Liu, J. Han, C. Li, J. Han, L. Can, *J. Phys. Chem. C* **2013**, *117*, 11584-11591.
19. Y. X. Feng, H. J. Wang, J. W. Wang, W. Zhang, M. Zhang, T. B. Lu. *ACS Appl. Mater. Interfaces* **2021**, *13*, 26573-26580.

20. B. Dubertret, P. Skourides, D. J. Norris, V. Noireaux, A. H. Brivanlou, A. Libchaber, *Science* **2002**, *298*, 1759-1762.
21. J. Aldana, N. Lavelle, Y. Wang, X. Peng, *J. Am. Chem. Soc.* **2005**, *127*, 2496-2504.
22. X. Zhang, Z. Wu, X. Zhang, L. Li, Y. Li, H. Xu, X. Li, X. Yu, Z. Zhang, Y. Liang, H. Wang, *Nat. Commun.* **2017**, *8*, 14675.
23. K. Wu, Z. Liu, H., Zhu, T. Lian, *J. Phys. Chem. A*, **2013**, *117*, 6362-6372.
24. J. Huang, J. D. Stockwell, Z. Huang, D. L. Mohler, T. Lian, *J. Am. Chem. Soc.* **2008**, *130*, 5632-5633.
25. K. Wu, H. Zhu, Z. Liu, W. Rodríguez-Córdoba, T. Lian, *J. Am. Chem. Soc.* **2012**, *134*, 10337-10340.
26. J. C. Phillips, *Rep. Prog. Phys* **1996**, *59*, 1133.
27. J. Nelson, S. A. Haque, D. R. Klug, J. R. Durrant, *Phys. Rev. B* **2001**, *63*, 205321.
28. J. Nelson, R. E Chandler, *Coord. Chem. Rev.* **2004**, *248*, 1181-1194.
29. J. K. Utterback, M. B. Wilker, D. W. Mulder, P. W. King, J. D. Eaves, G Dukovic, *J. Phys. Chem. C* **2019**. *123*, 886-896.
30. L. Lüer, G. Lanzani, J. Crochet, T. Hertel, J. Holt, Z. V. Vardeny, *Phys. Rev. B* **2009**, 80, 205411.
31. T. Koyama, S. Shimizu, T. Saito, Y. Miyata, H. Shinohara, A. Nakamura, *Phys. Rev. B* **2012**, 85, 045428.
32. B. Gao, G. V. Hartland, L. Huang, *J. Phys. Chem. Lett.* **2013**, *4*, 3050-3055.
33. D. Sun, Z. K. Wu, C Divin, X. Li, C. Berger, W. A. de Heer, P. N. First, T. B. Norris, *Phys. Rev. Lett.* **2008**, *101*, 157402.
34. H. Wang, Y. Li, H. Wang, H. Dai, *Chem. Soc. Rev.* **2013**, *42*, 3088-3113.
35. Y. Liang, Y. Li, H. Wang, H. Dai, *J. Am. Chem. Soc.* **2013**, *135*, 2013-2036.
36. K. Sokołowski, J. Huang, T. Földes, J. A. McCune, D. D. Xu, B. de Nijs, R. Chikkaraddy, S. M. Collins, E. Rosta, J. J. Baumberg, O. A. Scherman, *Nat. Nanotechnol.* **2021**, *16*, 1121-1129.
37. S. Jiang, Z. Chen, X. Chen, D. Nguyen, M. Mattei, G. Goubert, R. P. Van Duyne, *J. Phys. Chem. C* **2019**, *123*, 9852-9859.
38. H. Z. Uzunmehmetoğlu, H. Y. Yenilmez, K. Kaya, A. Koca, A. Altındal, Z. A. Bayır, *Inorg. Chim. Acta Rev.* **2017**, *459*, 51-62.
39. A. Gök, E. B. Orman, Ü. Salan, A. R. Özkaya, M. Bulut, *Dyes Pigm.* **2016**, *133*, 311-323.
40. K. Mizuno, J. Ishii, H. Kishida, Y. Hayamizu, S. Yasuda, D. Y. Futaba, M. Yumura, K. Hata, *Proc. Natl. Acad. Sci. U.S.A.* **2009**, *106*, 6044-6047.

TOC

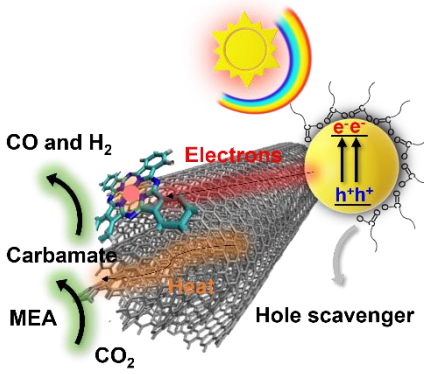

A ternary hybrid photocatalyst architecture is developed to convert amine-captured CO_2 to syngas with solar energy. The carbon nanotube plays key roles in transferring photoexcited electrons from the quantum dot to the molecular catalyst and in generating local heat from light irradiation for carbamate activation.

Keywords:

CO_2 reduction; photochemistry; ternary hybrid material; CO_2 capture; molecular catalyst